Influence of trapped and interfacial charges in organic multilayer light-emitting devices

Wolfgang Brütting, H. Riel, T. Beierlein, Walter Rieβ

Angaben zur Veröffentlichung / Publication details:

Brütting, Wolfgang, H. Riel, T. Beierlein, and Walter Rieβ. 2001. "Influence of trapped and interfacial charges in organic multilayer light-emitting devices." *Journal of Applied Physics* 89 (3): 1704–12. https://doi.org/10.1063/1.1332088.

Influence of trapped and interfacial charges in organic multilayer light-emitting devices

Cite as: Journal of Applied Physics **89**, 1704 (2001); https://doi.org/10.1063/1.1332088
Submitted: 01 August 2000 . Accepted: 19 October 2000 . Published Online: 17 January 2001

W. Brütting, H. Riel, T. Beierlein, and W. Riess

Influence of trapped and interfacial charges in organic multilayer light-emitting devices

W. Brütting[a)]
Experimental Physics II, University of Bayreuth, 95440 Bayreuth, Germany

H. Riel, T. Beierlein, and W. Riess
IBM Research, Zurich Research Laboratory, 8803 Rüschlikon, Switzerland

(Received 1 August 2000; accepted for publication 19 October 2000)

The influence of trapped and interfacial charges on the device characteristics of organic multilayer light-emitting devices is investigated. We have studied devices consisting of 20 nm copper phthalocyanine as buffer and hole-injection layer, 50 nm *N,N′*-di(naphthalene-1-yl)-*N,N′*-diphenyl-benzidine (NPB) as hole-transport layer, and 65 nm tris(8-hydroxyquinolinato)aluminum (Alq_3) as electron transport and emitting layer sandwiched between a high-work-function metal and a semitransparent Ca electrode. Current–voltage measurements show that the device characteristics in negative bias direction and at low positive bias are influenced by charges trapped within the organic layers. This is manifested by a strong dependence of the current on the direction and speed of the voltage sweep in this range. Low-frequency capacitance–voltage and static charge measurements reveal a voltage-independent capacitance in negative bias direction and a significant increase between 0 and 2 V, indicating the presence of negative interfacial charges at the NPB/Alq_3 interface. Transient experiments show that the delay time of electroluminescence under forward bias conditions is controlled by the buildup of internal space charges rather than by charge-carrier transport through the organic layers.
[DOI: 10.1063/1.1332088]

I. INTRODUCTION

Electroluminescence (EL) in organic solids requires several steps, including the injection, transport, capture, and radiative recombination of positive and negative charge carriers inside an organic layer with suitable energy gap, to yield visible light output. A very successful approach to optimize these individual steps separately is the concept of organic multilayer light-emitting devices (OLEDs) with heterostructures between different organic materials.[1,2] The simplest OLED of this kind consists of a heterostructure between a hole-conducting material (usually a triphenyl-amine derivative) and an electron-conducting aluminum chelate complex (Alq_3), where light emission is generated in the Alq_3 layer close to the organic–organic interface. As shown by the early work on molecular crystals, the relevant mechanism of EL in organic solids is injection-type luminescence, which has the consequence that the optimization of the yield in these devices requires high and equal densities of positive and negative carriers at the internal interface.[3–5]

A common starting point for device optimization is to consider molecular energy levels, namely the highest occupied and lowest unoccupied molecular orbitals, which are relevant for the magnitude of the energy barriers at the injecting contacts and at the organic–organic interface (see also Fig. 1). Although the knowledge of these energy levels is a prerequisite for choosing the right combination of organic materials and electrodes, it does not necessarily tell enough about the energetic situation in an operating device with high densities of injected charge carriers. This is because the accumulation of charge carriers as space charges can significantly modify the electrical potential inside the device. In the device under consideration, we can indeed expect to have space charges for several reasons. First of all, space charges can arise in the bulk of a single layer of a material if a contact is able to inject more carriers than the material has in thermal equilibrium.[6] This leads to space-charge-limited currents, which have been observed in various types of OLEDs.[7–10] In the presence of an organic–organic interface in a heterolayer device, the energetic level offset at the interface can be another source of the buildup of interfacial space charges. Even in the absence of these energetic barriers, the significant differences of charge-carrier mobilities for majority and minority carriers in the respective layers (see Sec. IV B) leads to the presence of mobility barriers at the internal interface, which in turn can be the source of interfacial space-charge formation. Clearly, knowledge of the charge and field distribution inside a device and of also its variation with the applied voltage is crucial for the physical understanding of device operation. Also, from the application perspective, knowledge of space charges is important for device optimization with respect to efficiency, temporal response, and long-term stability.

We present experimental evidence of the presence of space charges in metal anode/copper phthalocyanine (CuPc)/*N,N′*-di(naphthalene-1-yl)-*N,N′*-diphenyl-ben-

a)Author to whom correspondence should be addressed; electronic mail: wolfgang.bruetting@uni-bayreuth.de

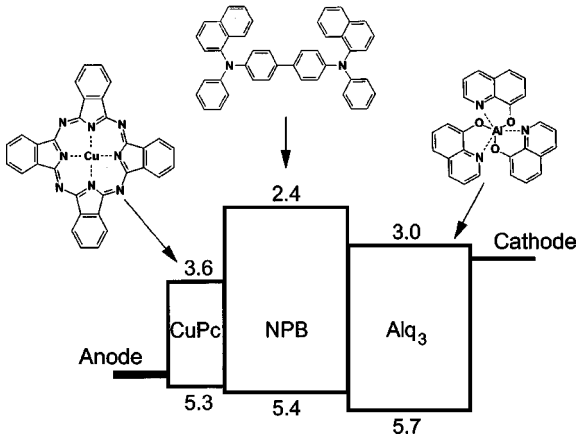

FIG. 1. Schematic energy-level diagram and chemical structures of the organic materials used for OLEDs.

zidine (NPB)/tris(8-hydroxyquinolato)aluminum (Alq_3)/Ca devices by current–voltage ($I-V$), capacitance–voltage ($C-V$), and transient EL measurements.

II. DEVICE PREPARATION AND EXPERIMENTAL METHODS

The devices were fabricated on glass substrates (Schott AF 45) precoated with a high-work-function anode such as indium–tin–oxide (ITO), Pt, Ir, Ni, or Pd ($\cong$75 nm thickness). The organic multilayer structure consists of 20 nm CuPc as buffer layer, 50 nm NPB as hole-transport layer, and 65 nm Alq_3 as electron-transporting and -emitting layer (see Fig. 1). In the case of a metal anode, EL was observed through a semitransparent 20-nm-thick Ca cathode. The active area of our devices was 2×3 mm^2. Prior to use, all organic materials were purified by vacuum train sublimation. Deposition of the organic materials was carried out in a high-vacuum system (Leybold) by thermal evaporation from resistively heated tantalum and tungsten boats. The base pressure in the chamber ranged between 4×10^{-7} and 1×10^{-6} mbar. Typical deposition rates were 1 Å/s. The evaporation chamber was attached directly to an argon glove-box system, which allowed devices to be fabricated, characterized, and encapsulated under inert conditions. $I-V$ and luminance–voltage characteristics were measured with a Hewlett Packard parameter analyzer (HP 4145B) and a Si photodiode (Hamamatsu S2281). The luminance calibration of the photodiode was obtained with a Photo Research PR704 spectroradiometer. Transient electroluminescence (TEL) was measured in a setup that allows the simultaneous detection of time-dependent EL as well as current and voltage across the device. The OLEDs were characterized in a customized HP 16 058 A test fixture with a Hamamatsu photomultiplier 5783-01 (time resolution $\cong$0.65 ns) located directly on top of the emitting area to detect EL intensity. A HP 8116 A pulse/function generator (50 MHz, rise time $\cong$7 ns, decay time $\cong$10 ns) was used to apply rectangular voltage pulses to the device. The pulse length was varied between 8 and 300 ms with a duty cycle of 0.1%–1%. Additionally, a dc offset voltage could be applied before the rectangular voltage pulse. The photomultiplier was connected to the 50 Ω input resistance of a digital oscilloscope (Tektronix 2440) to record the EL signal. A second digital oscilloscope (Tektronix 2440) allowed the voltage pulse and the time-dependent current flow through the device to be monitored simultaneously with the EL signal. $C-V$ measurements were carried out with a frequency response analyzer (Solartron Instruments SI1260). Typically, the oscillator level was set to 50 mV, and the measurement averaged over 100 cycles of the respective frequencies. Static discharge measurements were performed with a Keithley electrometer EM 617. Charging of the OLED was performed for a duration of 1 min by the built-in voltage source of the electrometer. Directly after charging, the device was separated from the source and connected to the Coulomb input of the electrometer to measure the total stored charge of the OLED. Switching was done manually, and care was taken to achieve high electrical isolation. All measurements were performed with encapsulated devices at room temperature.

III. EXPERIMENTAL RESULTS

A. *I–V* characteristics

Figure 2 shows the dependence of $I-V$ and luminance–voltage characteristics on sweep direction and speed for a metal anode/CuPc/NPB/Alq_3/Ca device. In Fig. 2(a) the voltage was incremented in steps of 50 mV from -3 to 7 V and back again. Current and luminance were detected with the parameter analyzer set to medium integration time and the delay time between individual data points set to 0. In this mode the time required to acquire a single data point depends on the magnitude of the detected current and ranges from 10 to 100 ms for the given device. Figure 2(b) was measured with long integration time and an additional delay of 10 s between individual data points. In both cases the current increases significantly in the forward bias direction above a threshold voltage of 2 V and is virtually unaffected at higher voltages by sweep direction and speed. The onset of EL determined at 10^{-4} cd/m^2 is 2.1 V and is not affected by external parameters. We note that the onset voltage for detectable EL is significantly lower than the optical gap of Alq_3 (2.7 eV) and corresponds instead to the built-in voltage (i.e., the difference in work function) of the two electrodes. Remarkable differences in the current flow are observed below 2 V, where no detectable EL and thus no double carrier injection takes place. The fast measurement shows a strong hysteresis between up and down sweeps [see Fig. 2(a)]. Importantly, the voltage where the current passes through zero is not at zero bias but at about -1.4 V for increasing voltage and about $+1.9$ V for the other sweep direction. Furthermore, under these measuring conditions, a step-like structure at about 0.5 V is observed in both sweep directions, which is characteristic for a multilayer structure containing CuPc. We do not observe this feature if the CuPc layer is omitted. The delay time of 10 s between subsequent data points used in the slow measurement is sufficient to achieve zero crossing of the current at 0 V [see Fig. 2(b)]. In addition the structure at about 0.5 V disappears. During these measurements we observe a higher current for decreasing voltage between 2 and 0.5 V and below -1 V. In these regimes the current is

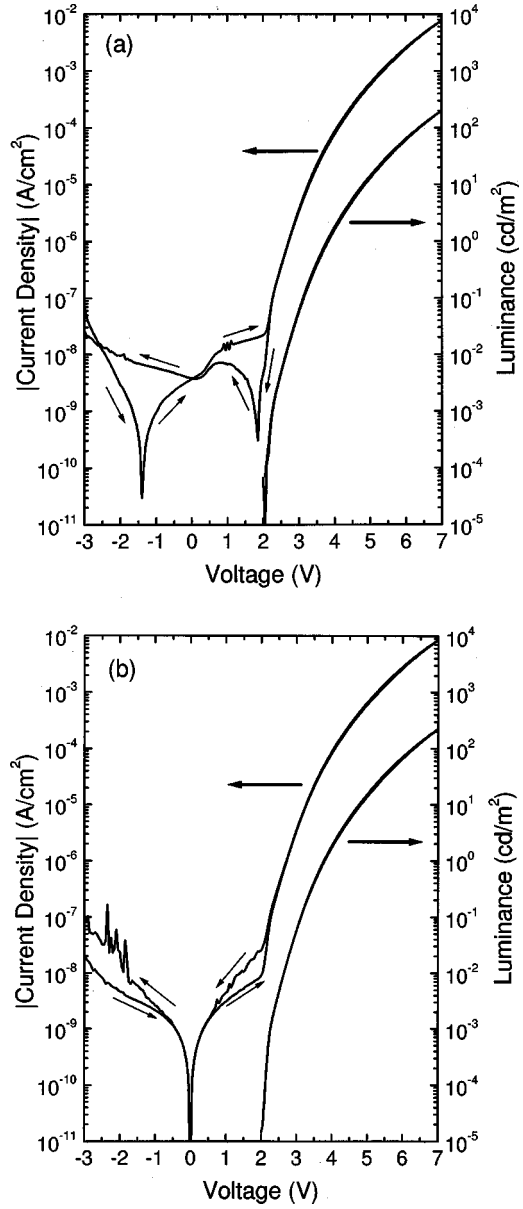

FIG. 2. Current–voltage and luminance–voltage characteristics of a metal anode/CuPc (20 nm)/NPB (50 nm)/Alq_3 (65 nm)/Ca device measured in different sweep directions and with different delay and integration times between individual voltage steps: (a) medium integration time and no delay time, (b) long integration time and 10 s delay time.

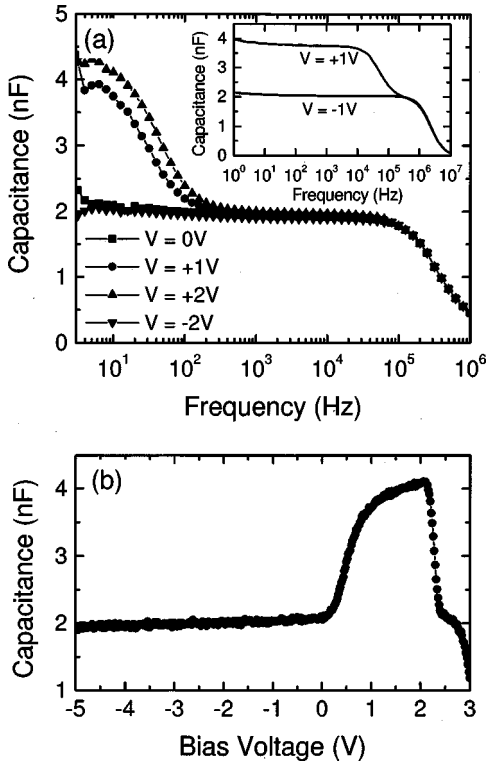

FIG. 3. Dependence of the capacitance on frequency and applied bias of the same device as in Fig. 2. The inset shows the frequency dependence of an ITO/NPB/Alq_3/Ca device for two bias values (from Ref. 34).

also relatively noisy. This is most likely caused by leakage currents, which can occur after operation of the device for longer times at higher positive bias.

The observation of such hysteresis effects in the $I-V$ characteristics is a hint of the presence of trapped charges in the device, which can require high time constants for the device to reach equilibrium after the voltage has been changed, especially in the bias regime below 2 V, where the device resistance ($R=V/I$) is extremely great.

B. Bias-dependent capacitance

The measurement of bias- and frequency-dependent device capacitance is a well-established technique for the investigation of conductivity, doping concentration, and trap states in organic semiconductors. For some polymeric semiconductors this method has been used to prove the existence of *p*-type doping leading to Schottky junctions with low-work-function metals.[11–13] Furthermore, in combination with temperature-dependent measurements, the energy of shallow acceptor states and deep trap states has been determined.[14] The materials used in this study, especially NPB and Alq_3, are expected to have very few intrinsic carriers and extrinsic dopants. In addition, they have been purified before usage. Only CuPc is known to be easily doped by atmospheric oxygen leading to *p*-type conducting behavior.[15] Thus, in the absence of free or trapped charges inside the device, we expect to measure a bias- and frequency-independent device capacitance corresponding to a series of three dielectric media with dielectric constants $\varepsilon_{r,i}$, thickness d_i, and area A. Given the active device area and the thickness of the individual layers together with the dielectric constants of the materials in the range from 3.5 to 4, one can estimate the device capacitance to be about 1.5–2 nF.

Figure 3 shows the differential capacitance $C=dQ/dV$ as a function of frequency of the same device as in Fig. 2 for a different applied bias and as a function of bias for a fixed frequency of 10 Hz. The frequency-dependent measurements in Fig. 3(a) show that at zero and negative bias the capacitance is essentially frequency-independent up to 10^4 Hz with a value close to 2 nF as estimated above. Above 10^5 Hz, the capacitance drops rapidly to a value much lower than the one corresponding to the materials' dielectric constants. This can be ascribed to parasitic effects due to lead/contact resistances and capacitances, which will not be discussed further here.

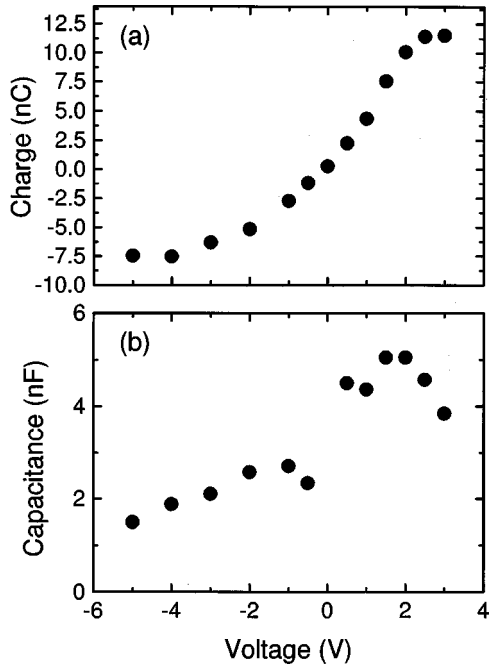

FIG. 4. Measured charge and calculated capacitance of the same device as in Fig. 2 after applying a different voltage for about 1 min.

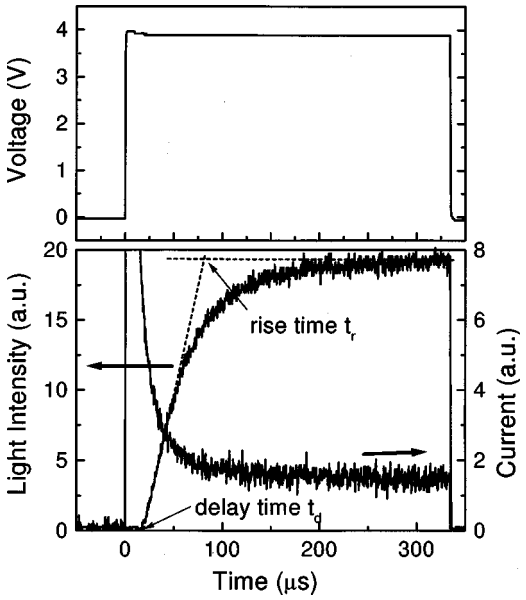

FIG. 5. Typical signals obtained in transient electroluminescence and current measurements after application of a rectangular voltage pulse. The method used to determine the delay and rise time is indicated.

The frequency dependence of the capacitance is almost identical for all applied bias values above about 200 Hz. Below 200 Hz and for positive bias (1 and 2 V), an increase in the capacitance is observed. At low frequencies ($f<10$ Hz) the capacitance appears to saturate at a value depending on the bias.

To study the bias dependence in more detail, the applied bias was varied at a fixed frequency of 10 Hz. This frequency is in most cases low enough to monitor the saturation value of the capacitance at low frequencies and still yield a good signal-to-noise ratio. The curves shown in Fig. 3(b) were taken from -5 to 3 V in steps of 25 mV with an additional delay of 10 s between the data points. No difference was observed for the opposite sweep direction. Whereas there is only a very weak bias dependence in the negative bias range, the capacitance increases significantly for positive bias at about 0.2 V and reaches a maximum at 2.1 V, which coincides with the onset of EL. Above this voltage the capacitance decreases sharply to a value of about 2 nF before it finally drops further as the bias exceeds 2.5 V. Note that in the regime of double carrier injection accompanied by recombination, the capacitance is not well defined, and thus no measurements for voltages above 3 V have been performed.

To determine the low-frequency saturation value of the device capacitance we have performed static discharge measurements. Figure 4 shows the measured charge Q for various charging voltages V and the capacitance calculated using the relation $C=Q/V$. Although the scattering of data is considerable, it is clear that the capacitance in positive bias direction increases and reaches a maximum at 2 V with a value about twice as high as for negative bias. At 2 V, the maximum value of 5 nF is slightly higher than that obtained in ac measurements, indicating that in the latter the capacitance has not reached its saturation value at the frequency of 10 Hz used here. In negative bias direction the capacitance has approximately the same constant value of 2 nF as in the ac measurement. The slight decrease with increasing negative bias can be explained as resulting from leakage currents that lead to a partial discharge while we switched between the voltage source and the Coulomb meter. Consequently, the measuring error increases with increasing negative voltage.

C. Transient EL

In TEL measurements one is interested in the time-resolved EL response to a pulse excitation, usually a rectangular voltage pulse. Figure 5 shows typical current and EL signals upon excitation with a rectangular voltage pulse (4 V). The EL signal is characterized by a finite delay between the application of the voltage pulse and the first appearance of EL, an extrapolated rise time to reach a steady-state value, and finally the plateau value itself. The time-dependent behavior of the current is characterized by a fast initial decrease from a high starting point to the steady-state value, which corresponds to the current in the $I-V$ characteristics at the given voltage. (The cutoff in Fig. 5 is caused by the limited dynamic range of the oscilloscope.) The initial decrease of the current also contains the charging current of the device. However, this process is expected to be much faster than the observed decay. Given the device capacitance of 2 nF and a series resistor of 100 Ω for $V\leqslant 5$ V (and 10 Ω for $V>5$ V) to measure the current, the resulting charging current should have decayed after roughly 5 RC time constants, yielding only about 1 μs (or 0.1 μs) for this process.

The observation of delayed EL has been used to extract charge-carrier mobilities and their field dependence in polymeric and organic LEDs.[16–20] Additional information about the kinetics of charge-carrier recombination and trapping can be obtained from the rise to the steady state and the decay of the EL signal after the voltage pulse has been switched off.

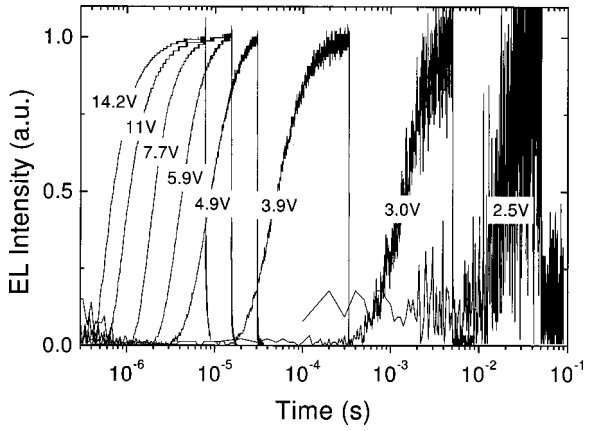

FIG. 6. Normalized transient electroluminescence signals for a metal anode/CuPc (20 nm)/NPB (50 nm)/Alq_3 (65 nm)/Ca device for voltage pulses with different amplitudes and lengths.

However, especially for multilayer structures, the interpretation of these transient experiments is not as straightforward as for a single-layer device because the injection of both types of carriers may not occur simultaneously.[21]

Figure 6 shows normalized TEL traces for voltage pulses with different amplitude and duration on a logarithmic time scale. The high sensitivity of the setup allows us to detect TEL with a reasonably good signal-to-noise ratio at a pulse amplitude of as low as 2.5 V, which is only 0.4 V higher than the onset voltage detected in dc measurements. At this voltage the delay time is almost 10 ms. It becomes rapidly shorter with increasing pulse amplitude and is only 3 μs at a voltage of 5 V, i.e., about three orders of magnitude lower. At 14.2 V (the highest voltage accessible with the pulse generator used), the delay time is less than 500 ns. The dependence of the delay and rise times determined as defined in Fig. 5 on the applied voltage is shown in Fig. 7. It is remarkable that the delay and rise times vary over more than 3 orders of magnitude in a narrow voltage range between 2.5 and 5 V.

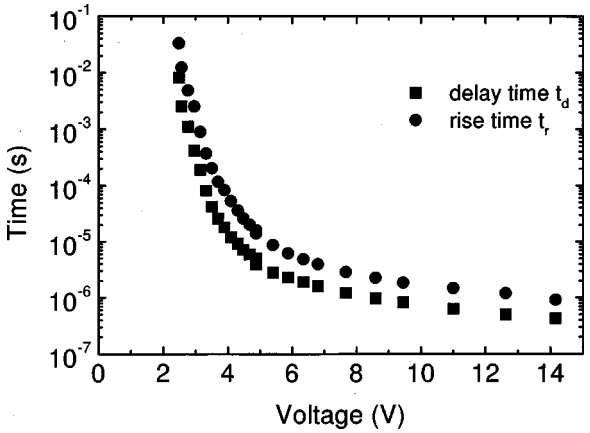

FIG. 7. Delay and rise time vs applied bias obtained from transient electroluminescence signals shown in Fig. 6.

IV. DISCUSSION

In the following discussion we are mainly interested in the role of the NPB/Alq_3 interface for the electrical characteristics of a large family of OLEDs incorporating both of these materials or derivatives thereof. Therefore we will treat the devices under investigation as bilayer systems composed of a hole-conducting and an electron-conducting compartment and having only one organic–organic interface, which is the NPB/Alq_3 interface. Thus we do not explicitly take into account the fact that, for reasons of device reliability and lifetime, the hole-transporting layer actually consists of two layers, namely CuPc and NPB, and therefore has another organic–organic interface. Where necessary, we will mention the peculiarities of this second interface separately.

A. Steady-state characteristics

From the $I-V$ and luminance–voltage characteristics shown in Fig. 2 it is immediately obvious that the operating voltage range of the OLEDs of interest can be divided into two regimes. These are the forward-bias regime ($V>2$ V), where light emission is observed and current flow is orders of magnitude higher than in the second region ($V<2$ V), where no light is emitted. The threshold voltage of 2 V is determined by the built-in voltage V_{BI}, which is the contact potential difference of anode and cathode (ignoring interface dipoles at the electrodes). In a fully depleted device the external voltage must overcome the resulting built-in voltage before a net drift current can flow. Therefore the relevant quantity is not the applied voltage V but rather the corrected effective value $V-V_{\mathrm{BI}}$.[22] In our case we independently estimated a V_{BI} of about 2 V by measuring the maximum open-circuit voltage of illuminated samples.

The observed dependence of the current on sweep speed and direction indicates that extremely slow processes are involved. Numerical simulations on NPB single-layer devices by Nguyen *et al.* show that the hysteresis observed in the $I-V$ characteristics can be explained qualitatively by the presence of deep traps, which require high time constants for reaching thermal equilibrium after a variation of the voltage across the device.[23]

A crucial point for a more quantitative understanding of the device characteristics is therefore the knowledge of the electric field distribution inside the individual layers. This is of overall importance because the hole-conducting (NPB) and electron-conducting materials (Alq_3) of this device have quite different charge-carrier-transport properties. NPB and related triphenyl-amines are purely hole-conducting materials with relatively high hole mobilities and very weak dependence of the mobility on the electric field F [$\mu_{h,\mathrm{NPB}}=6.1\times10^{-4}\,\mathrm{cm^2/V\,s}\cdot\exp(1.5\times10^{-3}(\mathrm{cm/V})^{1/2}\cdot\sqrt{F})$], whereas Alq_3 exhibits predominantly electron transport with lower carrier mobilities and a strong electric field dependence [$\mu_{e,\mathrm{Alq_3}}=7.1\times10^{-10}\,\mathrm{cm^2/V\,s}\cdot\exp(1.2\times10^{-2}(\mathrm{cm/V})^{1/2}\cdot\sqrt{F})$].[24,25] On the other hand, recent investigations by time-of-flight and TEL have shown that hole transport in Alq_3 is also not negligible, although its low-field hole mobility is considerably lower than the values for electrons [$\mu_{h,\mathrm{Alq_3}}=6\times10^{-11}\,\mathrm{cm^2/V\,s}\cdot\exp(9\times10^{-3}(\mathrm{cm/V})^{1/2}$

$\cdot\sqrt{F})]$.[26,27] Owing to the strong field dependence of the charge-carrier mobility of holes and electrons in the Alq_3 layer, the time scale to reach a stationary charge distribution depends strongly on the electric field distribution in this layer. A further point concerns the injection of carriers from the electrodes into the organic layer and from one organic layer into the adjacent one, where the electric field in the individual layers and at the interfaces also plays an important role.

To a first approximation one can assume from the energy-level diagram of the OLED shown in Fig. 1 that the voltage drops homogeneously over the entire device. As NPB and Alq_3 have similar dielectric constants, the electric field in the hole- and electron-conducting layers is given by $F^{(a)}=(V-V_{BI})/d_{tot}$, where d_{tot} is the total thickness of both organic layers. The capacitance in this case is $C^{(a)}=\varepsilon_r\varepsilon_0 A/d_{tot}$, where A is the device area. However, such a situation is not very realistic for the OLED operated under a forward bias condition, because from the large difference in hole and electron mobility in NPB and Alq_3, respectively, one has to expect that most of the applied voltage will drop at the Alq_3 layer. Indeed, recent electroabsorption measurements by Rohlfing *et al.* have shown that the voltage drop at the Alq_3 layer for positive bias is almost ten times greater than at the NPB layer.[28] Thus the electric field in the NPB layer is virtually negligible as compared to the field in the Alq_3 layer: $F^{(b)}_{NPB}=0$ and $F^{(b)}_{Alq}=(V-V_{BI})/d_{Alq}>F^{(a)}$. Such a discontinuity in the electric field must be accompanied by an accumulation of charge carriers at the interface (the simplest case being in an infinitely thin layer) via

$$\Delta F=\frac{\sigma}{\varepsilon_r\varepsilon_0}, \tag{1}$$

where σ is the interfacial charge density, and equal dielectric constants ε_r in both materials are assumed. The capacitance is now determined by the Alq_3 thickness alone and, at $C^{(b)}=\varepsilon_r\varepsilon_0 A/d_{Alq}$, is greater than $C^{(a)}$.

From our $C-V$ measurements (see Fig. 3) we can indeed see that there is a transition from a situation similar to case (a), where the capacitance is equal to the geometrical capacitance of the device for $V<0$ V, to the situation in case (b) for V approaching 2 V. In the latter case the capacitance is about twice as high as in the reverse bias direction, which corresponds well to the thickness of the Alq_3 layer of 65 nm compared to about 70 nm for the sum of the CuPc and NPB layer thicknesses. By systematically varying the thickness of both organic layers in ITO/NPB/Alq_3/Ca devices, Berleb *et al.* have recently found that the value of the capacitance in reverse bias direction always corresponds to the total thickness of all organic layers, whereas the value at 2 V is determined solely by the thickness of the Alq_3 layer.[29] The increase in the capacitance at a voltage well below the built-in voltage was attributed to the presence of negative charges at the NPB/Alq_3 interface, resulting in a discontinuity of the electric field as discussed above. Our $C-V$ measurements also prove that under sufficiently large negative bias the device behaves like a dielectric with no mobile charges inside the organic layers. The weak voltage dependence of the capacitance observed in this range can be attributed to the presence of the CuPc layer (presumably some residual doping) and is not seen if this layer is omitted. When the bias voltage is increased above 0 V, the capacitance increases, indicating that the NPB layer has reached the flatband condition and its resistance drops drastically.[29] With increasing bias, holes are injected from the anode and gradually reduce the immobile negative charges at the NPB/Alq_3 interface. At V_{BI} the negative interfacial charge is fully compensated and the device is in the flatband condition. The additional positive charges inside the device for $0<V\leqslant V_{BI}$ are directly measured in the discharge experiments shown in Fig. 4. An interesting point to mention is the critical voltage V_c at which the crossover from the dielectric to the charged state of the device is observed. This crossover occurs at a value of V_c that is given by the magnitude of the interfacial charge density σ and the thickness of the Alq_3 layer via[29]

$$\frac{V_c-V_{BI}}{d_{Alq3}}=\frac{\sigma}{\varepsilon_r\varepsilon_0}. \tag{2}$$

Using $V_c\approx 0$ V, $V_{BI}\approx 2$ V, and $\varepsilon_r\approx 3.5$, the interfacial charge density can be estimated to be $\sigma\approx -5.9\times 10^{11}$ e/cm^2, which is in good agreement with the value of $\sigma\approx -6.8\times 10^{11}$ e/cm^2 obtained on ITO/NPB/Alq_3/Ca devices.[29]

B. Transient response

The scenario described above has important consequences for the transient response of OLEDs, because the compensation of the negative interfacial charges cannot be expected *a priori* to occur instantaneously. This is directly seen in the frequency dependence of the capacitance, which shows that the enhanced capacitance between 0 and 2 V resulting from the redistribution of the electric field can only be monitored up to frequencies of about 200 Hz. Furthermore, in forward direction ($V>V_{BI}$) the electric field inside the Alq_3 layer and at the Alq_3/cathode interface is enhanced by the presence of the positive space charge at the NPB/Alq_3 interface. From this field enhancement at the cathode side one has to expect a strong influence on the electron-injecting properties of the cathode into Alq_3, even if the injection barrier is assumed to be small as in the case of Ca.

Transferring the scenario described above to TEL experiments, several processes have to occur subsequent to the application of a positive voltage pulse with $V>V_{BI}$ before light emission can take place: First the injection of holes, leading to a compensation of negative interfacial charges and the buildup of a positive space charge at the NPB/Alq_3 interface, and then the injection of electrons at the cathode and their transport to the NPB/Alq_3 interface, where they can ultimately recombine radiatively with holes injected from NPB into Alq_3. Therefore it is not as straightforward to obtain charge-carrier mobilities from the delayed onset of EL in these OLEDs as reported for single-layer devices (see, e.g., the detailed discussion of this issue in Ref. 20, where the transient response of Alq_3-based single- and multilayer devices is compared). The important question here is whether the observed delay and rise times (as defined in Fig. 5) originate from electron transport through the Alq_3 layer to the

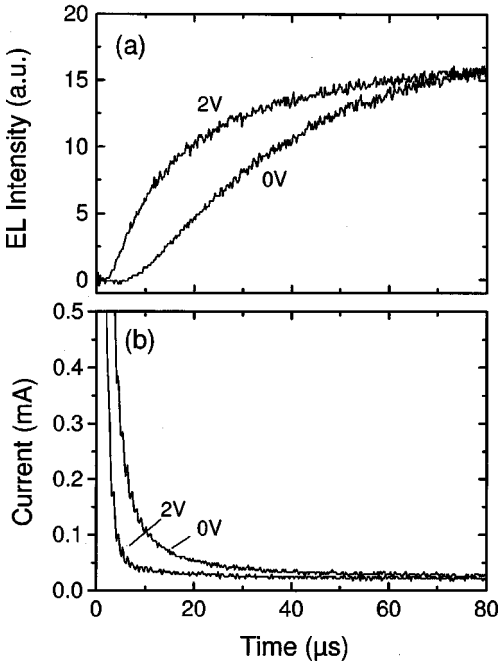

FIG. 8. Transient electroluminescence and current at a pulse height of 4 V for two different offset bias values.

recombination zone or from the buildup of the internal space charge and the concomitant redistribution of the electric field inside the device. A direct check whether the buildup of space charges contributes to the observed temporal response of the OLED can be obtained by superimposing a dc offset bias to the applied voltage pulse. Figure 8 compares two EL traces obtained with the same voltage amplitude of 4 V but different offset biases: 0 and 2 V. The bias value of 2 V is chosen just below the onset of double carrier injection to guarantee the compensation of negative charges at the NPB/Alq_3 interface, as has been proved by $C-V$ measurements. Figure 8 clearly shows that the delay and rise times of the EL signal to a steady-state value are at least a factor of 2 shorter if a positive bias of 2 V is applied prior to application of the 4 V pulse. This directly proves that the buildup of a space charge at the NPB/Alq_3 interface has a significant influence on the transient response of light emission in this OLED structure. Also the decay of the current to the steady state is much faster in the presence of the positive bias, which in turn shows that the initial high current and its decay with time after the application of a voltage pulse are not given by the RC time constant of the setup. Instead, this temporal behavior of the current directly reflects the buildup of the internal space charge in the device. As the buildup of a positive space charge in the NPB layer reduces the electric field in the vicinity of the hole-injecting contact, the initial current at $t=0$ in the absence of space charges is much higher than the steady-state current for $V>V_{\mathrm{BI}}$. By taking the integral of the current over time, one can directly estimate the accumulated charge injected into the device. The integration from $t=0$ to 100 μs yields a charge of 7.3 nC for zero offset bias and only 4.5 nC for 2 V positive bias. The difference of almost 3 nC is a crude estimate for the space charge builtup by the positive bias of 2 V prior to the voltage pulse. This is in the same range as the values measured directly in the discharge experiments [see Fig. 4(a)].

Bearing in mind that the buildup of space charges has a non-negligible influence on TEL, one can nevertheless use the delay and rise times obtained from the EL transients displayed in Fig. 6 to calculate charge-carrier mobilities in Alq_3. In our device structure, EL occurs when the leading fronts of opposite carrier packages meet in the Alq_3 layer close to the NPB/Alq_3 interface. At a given electrical field F and layer thickness d, the delay time t_d depends on the mobility μ as

$$t_d=\frac{d}{\mu\cdot F}. \tag{3}$$

If the mobilities of both charge-carrier types in Alq_3 are very different, instead of the ambipolar mobility $\mu=\mu_h+\mu_e$, the higher drift mobility will determine the delay time. From the delay time of the EL signal one can calculate the mobility by taking into account the built-in voltage as

$$\mu=\frac{d}{t_d\cdot F}$$

with

$$F=\frac{V-V_{\mathrm{BI}}}{d}. \tag{4}$$

As the mobility of holes in NPB is approximately 3 orders of magnitude higher than that of electrons in Alq_3 ($\mu_{h,\mathrm{NPB}}\gg\mu_{e,\mathrm{Alq_3}}$) and because most of the applied voltage drops at the Alq_3 layer as discussed above, it is reasonable to consider only the thickness of the Alq_3 layer in the calculation of the electrical field. Furthermore, owing to the higher mobility of electrons compared to that of holes in Alq_3 ($\mu_{e,\mathrm{Alq_3}}\gg\mu_{h,\mathrm{Alq_3}}$),[24,26,27] recombination takes place in the Alq_3 layer close to the NPB/Alq_3 interface. Thus the delay of EL will be determined by the transit time of electrons in the Alq_3 layer.

Using the measured delay and rise times (see Fig. 7) one can calculate a field-dependent electron mobility in Alq_3 as shown in Fig. 9. A plot of the logarithm of the mobility versus the square root of the electric field has been chosen because these disordered materials are known to show a field-dependent mobility of the form $\mu\propto\exp(\beta\sqrt{F})$.[30] This is explained by a disorder formalism[31,32] or the phenomenological Poole–Frenkel model.[33] The data in Fig. 9 show two regions with a significantly different behavior of log μ versus $\sqrt{F}$ with a crossover at about $\sqrt{F}=700\,(\mathrm{V/cm})^{1/2}$. In the low-field regime, a pronounced field dependence is observed and the calculated mobility varies over more than 2 orders of magnitude. This is followed by the second regime, where the determined mobility changes by a factor of only 2. The existence of two regions with different field dependences indicates that two limiting processes are involved in the temporal EL response of these multilayer devices.

By calculating the mobility from the experimental data we have so far neglected the influence of the internal interface on the transient response. As discussed above, space charges build up with time at the NPB/Alq_3 interface, which

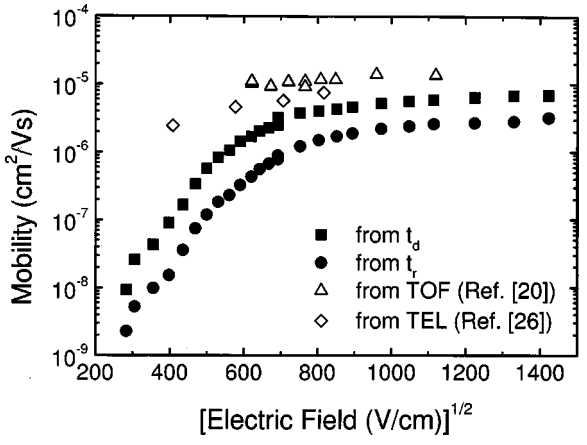

FIG. 9. Calculated mobility values according to Eq. (4) from the delay and rise times displayed in Fig. 7. To calculate the field, a built-in voltage $V_{BI}=2$ V was used. For comparison mobility data obtained by TOF on a 150-nm-thick Alq_3 layer (Ref. 20) and by TEL on an ITO/TPD (60 nm)/Alq_3 (60 nm)/Ca device (Ref. 26) are shown.

leads to an enhancement of the electric field in the Alq_3 layer and facilitates electron injection at the cathode. The time required for the space charge to build up depends on the applied voltage pulse (i.e., the amount of current flow). Consequently, if the buildup of the internal space charge takes significantly longer than the transit of electrons through the Alq_3 layer, the delay time will be determined by the former process and will hence contain no information about the electron mobility in Alq_3. Therefore, we attribute the marked increase of the calculated mobility in the low-field region to a charging effect at internal interfaces rather than to a real field-dependent behavior of the mobility.

This interpretation is supported by recent time-of-flight (TOF) measurements on thin (150 nm) Alq_3 layers, where data shown as open triangles in Fig. 9 were obtained. The values of the electron mobility from TOF are only weakly field dependent and are higher than the data from TEL in the entire range of the applied electric fields. Whereas the difference is only about a factor of 2 above $\sqrt{F}=700\,(\mathrm{V/cm})^{1/2}$, the mobility from TEL drops drastically below this value, and at $\sqrt{F}=200\,(\mathrm{V/cm})^{1/2}$ is about 3 orders of magnitude lower than the extrapolated TOF data. This again confirms that in the low-field regime the behavior is completely dominated by the buildup of the internal charge distribution rather than by charge-carrier transport.

The fact that the TEL response in heterolayer OLEDs can be controlled by the buildup of an internal space charge inside the device has been found experimentally and verified by numerical simulations on polymeric bilayer OLEDs by Nikitenko *et al.*[21] They have shown that the temporal response (delay and rise time of EL) depends very sensitively on the injection barriers of electrons and holes at the cathode and anode side, respectively. For sufficiently large injection barriers the buildup of the internal space charge can actually fully control the transient response of the device.

In the discussion so far we have neglected the presence of the CuPc layer as an additional hole-injection and buffer layer. However from a comparison of the work described here and investigations on ITO/NPB/Alq_3/Ca devices without a CuPc layer one can find characteristic differences in the frequency dependence of the capacitance[34] and the TEL response at low fields.[26] The corresponding curves are included in Figs. 3(a) and 9. In the bilayer device the enhanced capacitance for positive bias can be observed up to a relaxation frequency of about 50 kHz, whereas in the device discussed here it drops already at about 50 Hz [see Fig. 3(a)]. In TEL the low-field response is also considerably faster without the CuPc layer (see Fig. 9). Both observations indicate that the usage of CuPc as a buffer layer—although it improves device reliability and lifetime—deteriorates hole injection, at least at low forward bias. An explanation could be found in an additional energy barrier at the interface to NPB, as well as the possibility of *p* doping in CuPc by oxygen. Both issues could lead to an accumulation of positive carriers in the vicinity of the hole-injecting electrode, which would reduce the electric field at the anode and thus impede hole injection and transport to the NPB/Alq_3 interface. This interpretation is consistent with work by Aziz *et al.* and Matsumura and Miyamae, where a deterioration of hole injection from oxygen–plasma-treated ITO into NPB upon introduction of a CuPc buffer layer has been found.[35,36]

V. CONCLUSION

Our experimental results show that the electrical characteristics of organic light-emitting devices that incorporate hole-conducting triphenyl-amine derivatives (e.g., NPB) and aluminum hydroxy-quinoline (Alq_3) can be separated into three regimes. First, there is the forward-bias regime above the built-in voltage V_{BI} of approximately 2 V, where double carrier injection, transport, and radiative recombination in the Alq_3 layer close to the NPB interface occur. Second, for high reverse bias ($V \ll V_{BI}$), the devices behave like an insulating dielectric sandwiched between two metal electrodes. Our $C-V$ measurements show that there is a third regime between a critical value V_c that depends on the Alq_3 thickness ($V_c \approx 0$ V for a 65-nm-thick Alq_3 layer) and the built-in voltage. The observation of an enhanced device capacitance indicates the presence of negative interfacial charges at the NPB/Alq_3 interface, which become gradually compensated by injected holes as the built-in voltage is approached. The consequences of this are seen in the TEL response, which at low forward voltages is completely governed by the buildup of the internal space charge rather than by the transport of electrons through the Alq_3 layer.

ACKNOWLEDGMENTS

The authors thank S. F. Alvarado, S. Barth, S. Berleb, S. Karg, and A. G. Mückl for valuable discussions, and M. Tschudy for preparing the substrates. W. B. acknowledges financial support from IBM Rüschlikon for hosting his visit.

[1] C. W. Tang and S. A. Van Slyke, Appl. Phys. Lett. **51**, 913 (1987).
[2] C. W. Tang, S. A. Van Slyke, and C. H. Chen, J. Appl. Phys. **65**, 3610 (1989).
[3] W. Helfrich and W. G. Schneider, Phys. Rev. Lett. **14**, 229 (1965).
[4] M. Pope and C. E. Swenberg, *Electronic Processes in Organic Crystals* (Clarendon, Oxford, 1982).
[5] J. Kalinowski, J. Phys. D **32**, R179 (1999).

[6] M. A. Lampert and P. Mark, *Current Injection in Solids* (Academic, New York, 1970).
[7] C. Giebeler, H. Antoniadis, D. D. C. Bradley, and Y. Shirota, J. Appl. Phys. **85**, 608 (1999).
[8] S. Berleb, W. Brütting, M. Schwoerer, R. Wehrmann, and A. Elschner, J. Appl. Phys. **83**, 4403 (1998).
[9] P. W. M. Blom, M. J. de Jong, and J. J. M. Vleggaar, Appl. Phys. Lett. **68**, 3308 (1996).
[10] L. Bozano, S. A. Carter, J. C. Scott, G. G. Malliaras, and P. J. Brock, Appl. Phys. Lett. **74**, 1132 (1999).
[11] J. Kanicki, in *Handbook of Conducting Polymers*, edited by T. A. Skotheim (Dekker, New York, 1986), Chap. 17.
[12] D. M. Taylor, H. Gomes, A. E. Underhill, S. Edge, and P. I. Clemenson, J. Phys. D **24**, 2032 (1991).
[13] M. Meier, S. Karg, and W. Rieß, J. Appl. Phys. **82**, 1961 (1997).
[14] J. Scherbel, P. H. Nguyen, G. Paasch, W. Brütting, and M. Schwoerer, J. Appl. Phys. **83**, 5045 (1998).
[15] A. K. Hassan and R. D. Gould, J. Phys.: Condens. Matter **1**, 6679 (1989).
[16] C. Hosokawa, H. Tokailin, H. Higashi, and T. Kusumoto, Appl. Phys. Lett. **60**, 1220 (1992).
[17] H. Vestweber, J. Oberski, A. Greiner, W. Heitz, R. F. Mahrt, and H. Bässler, Adv. Mater. Opt. Electron. **2**, 197 (1993).
[18] S. Karg, V. Dyakonov, M. Meier, W. Rieß, and G. Paasch, Synth. Met. **67**, 165 (1994).
[19] H. Nakamura, C. Hosokawa, and T. Kusumoto, in *Inorganic and Organic Electroluminescence*, edited by R. H. Mauch and H.-E. Gumlich (Wissenschaft & Technik, Berlin, Germany, 1996), pp. 95–100.
[20] S. Barth, P. Müller, H. Riel, P. F. Seidler, W. Rieß, H. Vestweber, and H. Bässler, J. Appl. Phys. (to be published).
[21] V. R. Nikitenko, Y.-H. Tak, and H. Bässler, J. Appl. Phys. **84**, 2334 (1998).
[22] J. C. Scott, S. Karg, and S. A. Carter, J. Appl. Phys. **82**, 1454 (1997).
[23] P. H. Nguyen, S. Scheinert, S. Berleb, W. Brütting, and G. Paasch, Phys. Rev. B (submitted).
[24] R. G. Kepler, P. M. Beeson, S. J. Jacobs, R. A. Anderson, M. B. Sinclair, V. S. Valencia, and P. A. Cahill, Appl. Phys. Lett. **66**, 3618 (1995).
[25] T. Tsutsui, H. Tokuhisa, and M. Era, Proc. SPIE **3281**, 230 (1998).
[26] A. G. Mückl, S. Berleb, W. Brütting, and M. Schwoerer, Synth. Met. **111–112**, 91 (2000).
[27] S. Naka, H. Okada, H. Onnagawa, J. Kido, and T. Tsutsui, Jpn. J. Appl. Phys., Part 2 **38**, L1252 (1999).
[28] F. Rohlfing, T. Yamada, and T. Tsutsui, J. Appl. Phys. **86**, 4978 (1999).
[29] S. Berleb, W. Brütting, and G. Paasch, Organic Electronics (in press); (http://www.elsevier.nl/homepage/sak/orgel/papers.htm).
[30] P. M. Borsenberger and D. S. Weiss, *Organic Photoreceptors for Imaging Systems* (Dekker, New York, 1993).
[31] H. Bässler, Phys. Status Solidi B **175**, 15 (1993).
[32] D. H. Dunlap, P. E. Parris, and V. M. Kenkre, Phys. Rev. Lett. **77**, 542 (1996).
[33] W. D. Gill, J. Appl. Phys. **43**, 5033 (1972).
[34] S. Berleb, W. Brütting, and G. Paasch, Synth. Met. (in press).
[35] H. Aziz, Z. D. Popovic, N. X. Hu, A. M. Hor, and G. Xu, Science **283**, 1900 (1999).
[36] M. Matsumura and Y. Miyamae, Proc. SPIE **3797**, 283 (1999).